

Large inelastic response of polyurea-coated steel plates to confined blast loading

Chengjian Zhang¹, Ye Yuan^{1,2*}, Xuanxuan Su¹, P.J. Tan³, Qibo Zhang¹, Pengwan Chen^{1**}

¹*State Key Laboratory of Explosion Science and Technology, Beijing Institute of Technology, Beijing 100081, PR China*

²*Beijing Institute of Technology Chongqing Innovation Center, Chongqing 401120, PR China*

³*Department of Mechanical Engineering, University College London, Torrington Place, London WC1E 7JE, UK*

Abstract

The large inelastic deformation performance of monolithic steel and polyurea-steel laminate plates to confined blast loading is investigated through a combination of experiments and finite-element modelling. Emphasis is placed on elucidating how the location of the polyurea coating(s) and steel substrate, relative to the direction of loading, affects their inelastic deformation and the impulse and energy transfer to the laminate plates. Experimental results show that monolithic steel plate outperforms – using the maximum central deflection as a criterion – its equivalent polyurea-steel laminate of equal mass in confined blasts. Results from finite element simulations, which will be shown to be in good agreement with the experiments, will reveal that a longer response time for the polyurea-steel laminate attributes to the greater saturation impulse and, in turn, the increased deformation over its monolithic counterpart of equal mass. The internal energy of a laminate plate, unlike its monolithic equivalent, is found to increase even after reaching its maximum central displacement through further out-of-plane deformation that spreads out laterally. The impedance mismatch between the elastomer and steel will be shown to play a key role in the amplification, or attenuation, of the blast wave depending on the placement of the elastomer. A parametric study is performed to elucidate the influence of thickness ratio and mass per unit area on the blast performance of the laminate plates.

Keywords: Confined blasts, Retrofitting solution, Modelling, Impulse saturation

*Corresponding author

**Corresponding author

Email addresses: yuanye20@bit.edu.cn (Ye Yuan^{1,2}), pwchen@bit.edu.cn (Pengwan Chen¹)

1. Introduction

Thin-walled structural members are used in a significant number of structural applications: aircraft, storage tanks, bulkheads in ships and etc. Their survivability – defined as the ability to retain service functionality in the face of threats – to extreme load cases have received increased attention lately, such as the confined blast performance of thin metallic plates [1–4]. The intensity of a confined blast is often amplified [5] through multiple shock wave reverberations, leading to prolonged loading duration, caused by the effects of confinement [6]; consequently, more severe structural damage, compared to its free-air counterpart (or external blasts) of equal charge mass, is a natural concomitant of the confinement effect [7]. There exists a large body of literature devoted to the load characterisation [7–11] and the performance of monolithic metal plates [1, 2, 12–18] to confined blasts – the aim is to better understand this class of loading so that effective mitigation strategies can be developed. Retrofitting by spray-on elastomer coating [19], such as polyurea, is a potential mitigation strategy for existing structures [20, 21]. Polyurea is highly affordable, lightweight, ductile and abrasion-resistant that readily adheres to a metallic surface within a short curing time. The advantages of polyurea-steel laminate plates over its monolithic equivalent of equal mass are already well known for impulsive [22] and for free-air blast loadings [23]. To the best of the authors’ knowledge, the blast performance of polyurea-steel laminate plates has not been investigated in the context of confined blast to date, and is the subject of this paper.

A large body of literature [24–28] reported on the blast resistance of elastomer-metal laminate plates. The blast mitigation capability of the elastomer-metal laminate plate strongly depends on the relative coating location relative to the loading direction. A frontal polyurea layer could enhance the destructive effect of the blast, promoting instead of alleviating the failure of the steel substrate; and only when applying the polyurea onto the opposite of the loading face can the necking instability of the steel layer be effectively delayed [19, 25, 26]. The reason is that the stiffness of the frontal polyurea coating would increase substantially under compressive loading from the blast, which would lower the impedance mismatch to the steel layer leading to greater energy transfer to the substrate [29]; whereas the rear polyurea coating would increase the effective tangent modulus of the laminate plate, resulting in deformation reduction and failure retardation in the steel substrate [30]. Recent study in [26] further added that the frontal coating could be melted and causes the loss of structural integrity caused by the heat generated by the fireball, whereas the rear polyurea coating is unaffected by the high temperature which can develop membrane action and contribute to the deformation reduction of the laminate plate. Notwithstanding, it remains unclear whether a polyurea-steel laminate plate offers significant advantage over its monolithic counterpart of equal mass owing to conflicting reports. On the one hand, the external blast resistance of non-blast-receiving face coated steel plate was reported by Hou et al. [25] to have superior performance over its equivalent monolithic steel counterpart; on the other hand, experimental study by Ackland et al. [24] showed that monolithic steel plates were able to dissipate the blast energy more efficiently, resulting in lower residual deformation compared to polyurea-steel laminate plates of equal mass.

In an external blast, three distinct modes of deformation can develop in fully-clamped monolithic metal plates: mode I - large inelastic deformation; mode II - tensile-tearing at the support and deformation; mode III - shear-band localisation at the support [31, 32]. For polyurea-steel laminate plates under impulsive [19, 29] and localised (near-field) external blast [23–25], they develop localised failure (in addition to the aforementioned mode I response) as follows: spalling of the polyurea coating, capping, petalling, debonding, and tensile tearing at the central region. It must be emphasized that the pulse-pressure loading arising from a confined blast is neither impulsive [5] nor localised [2]. Numerical predictions by Yuan et al. [2] have shown that, at a small standoff distance, the blast load impinging on the target is only initially localised for a short duration; for the most part, the loading is nearly uniformly distributed over the target due to the effects of confinement by the blast chamber. Hitherto, an in-depth study into the confined blast response of polyurea-steel laminate plate is still lacking; a thorough understanding of how the confined loading conditions affect the large inelastic response of the laminate plate and how it, in turn, induces different localised failure modes is critical to their successful implementation as a retrofit solution.

The focus of this paper will be on the mode I inelastic response of the laminate plate – as part of an wider on-going investigation – since this is critical to elucidating the mechanism that induces the different modes of localised failure that will develop subsequently. It aims to characterise the mode I deformation of polyurea-steel laminate plates to confined blast loading; and to elucidate how different coating location (proximal, distal or both), relative to the direction of the incident blast load, affects load transfer, energy absorption and blast wave dissipation. Details of the experiments are first described and the experimental results presented. The mass of the explosive charge was carefully chosen so that the laminate plate only developed large inelastic deformation (mode I) without inducing any of the subsequent localised failure modes. Experimental data for the temporal central deflection were recorded and compared to predictions from three-dimensional finite element (FE) simulations. The FE model was used to infer the interface pressure versus time history impinging on the plates; and, the validated model used to provide further insights into the impulse and energy transfer, the equivalent strain field, velocity and deformation profile that were difficult to measure experimentally. A parametric study was also conducted to investigate the effects of coating thickness ratio and area density on the mode I performance of the laminate plates.





2. Experiments

2.1. Specimens

Table 1 lists four different target configurations that were tested: (1) a monolithic steel plate (S); (2) a steel plate with distal polyurea coating (S-P); (3) a steel plate with proximal polyurea coating (P-S); (4) a steel plate with both proximal and distal polyurea coatings (P-S-P). The first letter in each abbreviation indicates the material (either steel or polyurea) facing the incoming blast load. All targets had identical overall in-plane dimensions of 0.4×0.4 m and area density of 12.83 kg/m^2 . The exposed plate area to the blast was 0.3×0.3 m. Notice that the above design of specimen took inspiration from the published literature:

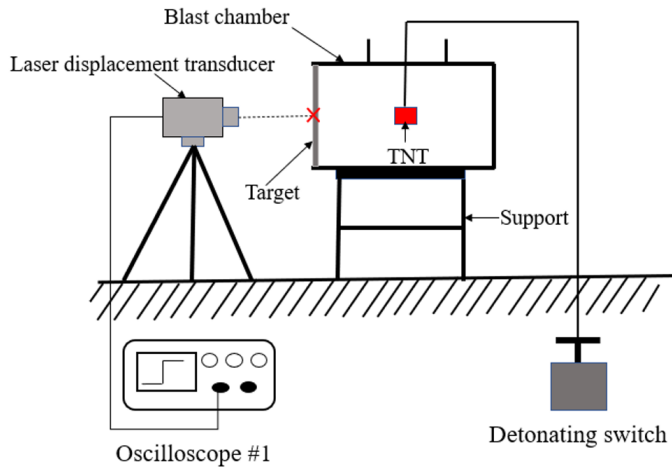
current area density is close to that in [19, 23, 25] and the current thickness ratio (polyurea over steel) is similar to that in [19, 24].

Table 1: Summary of target configurations.

Target structure	Loading scenario	Thickness (mm)			Area density (kg/m ²)
		Polyurea	Steel	Total	
S		0	1.65	1.65	12.83
P-S		4	1	5	12.83
S-P		4	1	5	12.83
P-S-P		2+2	1	5	12.83

P and S stands for polyurea and steel, respectively.

2.2. Blast tests



(a) Sketch of experimental setup



(b) Photo of experimental setup

Figure 1: Experimental setup of the confined blast tests.

Figure 1 shows the assembly of the test rig, which consists of a stiff blast chamber, a blanking plate, flanges and the target structure. The overall dimension of the blast chamber is $400 \times 400 \times 800$ mm. The blast chamber had a square opening of 300×300 mm at each end. The chamber was welded to the top of a supporting metal frame as shown in Fig. 1b. A heavy-weight metal box was added to the supporting frame to prevent rigid body motion of both the supporting frame and the blast chamber during the blast tests. The plate specimens were clamped along their edges between the flange and the support frame of the blast chamber, through $12 \times \phi 20$ mm bolts. The other end of the blast chamber was sealed off by clamping a 10 mm thick blanking plate, made of hardened steel, in a similar fashion. The cylindrical TNT charge ($25 \times \phi 25$ mm, as shown in Fig 1a) was hung by a wire from a $\phi 60$ mm vent hole (located at the top of the blast chamber) so that it is located at the centre of the blast chamber. The standoff distance between the target and the explosive was 400 mm. In total, four tests were performed. A constant TNT mass of 10g was used for each target configuration. A laser displacement sensor (Fig. 1b) was used to measure the transient out-of-plane central deflection of the non-blast-receiving-face of the target plate, and the measurements were used to validate the numerical model. The internal pressure was not measured during the test; however, the peak over-pressures and maximum transmitted impulses can be easily inferred from the validated numerical model.

2.3. Experimental results

Figure 2 shows that the monolithic steel plates and polyurea-steel laminate plates under confined blast loading were dominated by large inelastic deformation. No localised damage, viz. spalling of polyurea coating, capping, petalling, debonding, and tensile tearing in the central region, as reported previously in [23, 25], were observed in the current experiments. It must be emphasized that the mass of the TNT charge was deliberately chosen so that it was just sufficient to induce mode I deformation, without localised damage, in all of the target configurations. Plastic hinge lines, in the form of a pyramidal profile, were clearly visible on the non-blast-receiving face of each target.

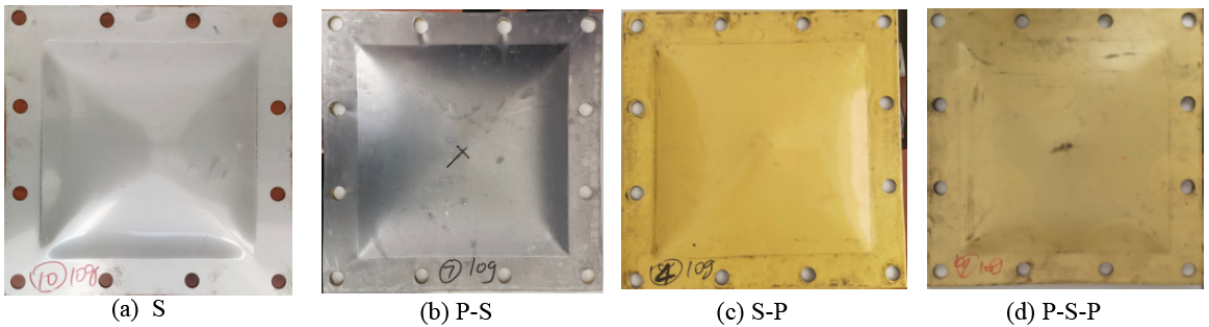


Figure 2: The distal (non-blast-receiving) face of the deformed target plates.

Figures 3 compares the maximum out-of-plane deflection between different target configurations. The monolithic steel plate had the smallest permanent out-of-plane deflection

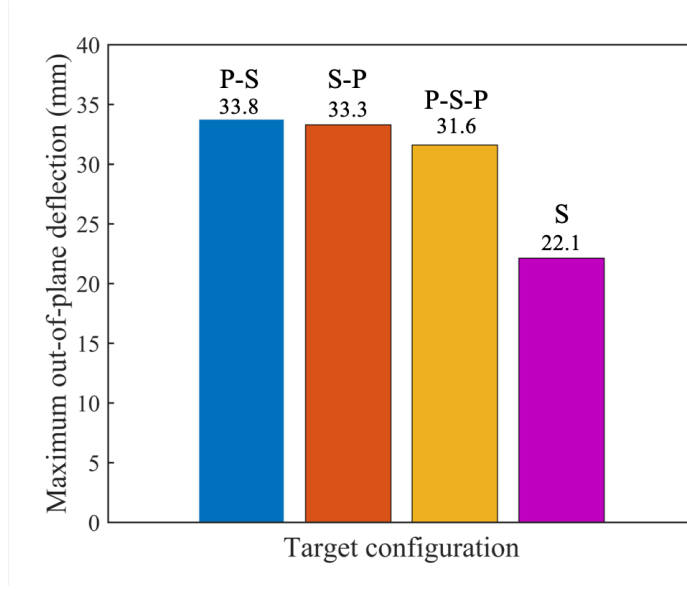


Figure 3: Maximum out-of-plane deflection measured in experiments.

compared to all the other laminate plates with equal mass – this agrees with the experimental findings by Ackland et al. [24]. It is evident that the polyurea coating(s), regardless of the surfaces to which were applied, did not lead to improved mode I blast performance when the results were compared on an equal mass basis. For polyurea-steel laminate plates, their out-of-plane deflection is insensitive to whether the polyurea applied to either one (proximal or distal) or to both sides of the steel plate. The inferior performance of the proximal coated plate compared to the distal coated one as reported in the literature [19, 25, 26] was not observed in the current experiments.

3. Numerical model development

Important field quantities that influence the overall structural response of the laminate plates, such as impulse and energy transfer, distribution of the confined blast load, deformation profile and equivalent plastic strain distribution, are difficult, if not impossible, to measure directly in the blast tests. Instead, they will be obtained from the validated numerical models. The confined blasts were simulated using the commercial software package ANSYS/LS-DYNA® 2020. The aforementioned field quantities, are compared for the different target configurations. A parametric investigation will also be performed to investigate the influence of the polyurea coating to plate thickness ratio, and the mass per unit area upon the maximum out-of-plane deflection of the different target configurations.

3.1. Arbitrary Lagrangian-Eulerian (ALE) simulation

Figure 4 shows the setup of the numerical model. The Arbitrary Lagrangian-Eulerian (ALE) scheme was adopted to capture the fully-coupled fluid-structure interactions between the Lagrangian (flange, blast chamber, bolt and plates) and Eulerian (air and explosive) meshes.

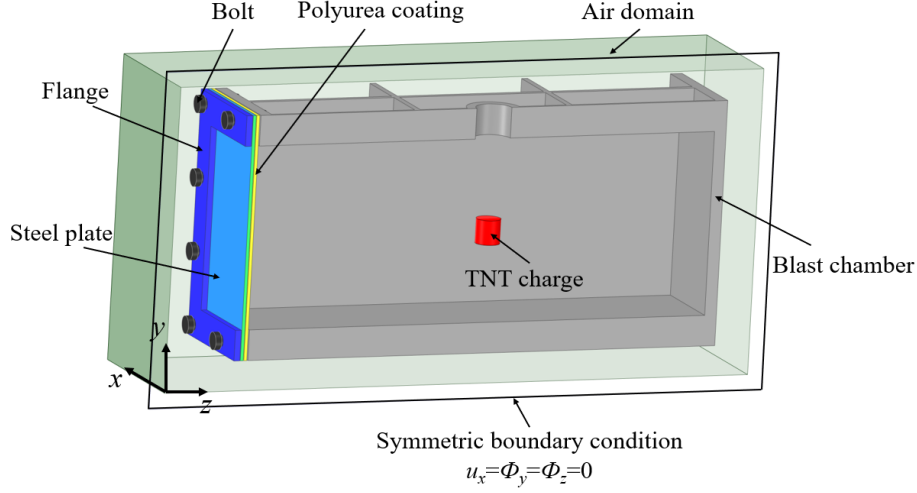


Figure 4: Schematic of the numerical model.

The air domain had a dimension of $300 \times 600 \times 1000$ mm, which extends beyond the blast chamber to allow for the deformation of the target plate. Three-dimensional (3D) eight-node solid brick elements with a unit aspect ratio and an element length of 5 mm were used to discretise the air domain. Mesh dependency studies confirmed that this grid size is sufficient to achieve an efficient coupling between the Eulerian and the Lagrangian elements. The air domain was modelled using an ideal gas law, with standard air properties. The Jones-Wilkins-Lee (JWL) EOS was used to simulate the cylindrical explosive. Tables 2 and 3 list the air properties, EOS properties and the detonation parameters. The steel plate and polyurea coating were discretised using four-node shell elements [2–4] and eight-node solid brick elements [23, 24, 26], respectively. The interface between plate and coating have matching meshes. At least four elements were used along the thickness direction (z -axis in Fig. 4) of the polyurea coating, which corresponds to an element height of 1 mm. Mesh sensitivity studies revealed that using elements of 4×4 mm² are sufficiently fine to yield mesh-independent predictions of the out-of-plane central deflection. No evidence of debonding between the polyurea coating and the steel substrate was observed during the post-test inspection of the plate specimens. Hence, a permanent bond between the polyurea coating and the steel substrate is assumed in the numerical models. This is achieved through a *tied contact* in LS-DYNA, i.e. there is no relative motion between the two surfaces that are in contact. The walls of the blast chamber and blanking plate were modelled as rigid plates by following the same in [3]. All the simulation was run for over 2.5 ms which was shown to be sufficiently long to model the entire elasto-plastic response of the structures.

3.2. Boundary conditions

Taking advantage of symmetry, only one-half of the entire set-up need to be modelled. A ‘flow-out boundary’ condition was applied to the boundaries of the Euler domain excluding the symmetric plane, which permits gaseous products to propagate beyond the Euler domain. The exact boundary condition was replicated in the current numerical simulations by

Table 2: Properties of air used in the simulations [2].

ρ_a	e_a	p_a	γ_a
(kg/m ³)	(KJ/Kg)	(Pa)	
1.225	206.8	104761	1.4

Table 3: Properties of the explosives in the simulations [2].

ρ_0	D	P_{CJ}	C_1	C_2	r_1	r_2	ω
(kg/m ³)	(m/s)	(Pa)	(Pa)	(Pa)			
1630	6930	2.10E+10	3.74E+11	3.75E+9	4.15	0.9	0.35

considering the flanges and the bolts. They were both modelled as rigid bodies with eight-node solid brick elements. The bolts were fully constrained to mimic the clamped boundary conditions in the experimental set-up. An automatic surface-to-surface contact was used to model the contact between the target plate and the clamps by following the numerical setup in [1, 2].

3.3. Constitutive models of steel and polyurea

The Johnson-Cook (JC) material model was used to model the 304 stainless steel plate, which has an equivalent stress σ_{eq} given by

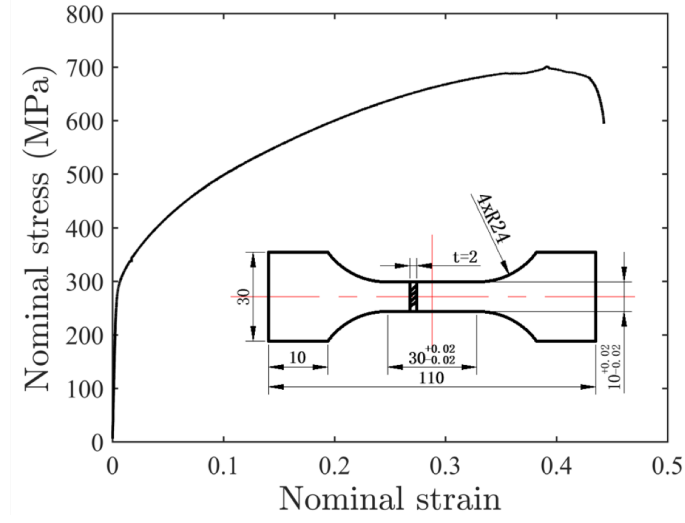
$$\sigma_{eq} = (A + B\epsilon_{eq}^n)(1 + C\ln\dot{\epsilon}_{eq}^*)(1 - T^{*m}) \quad (1)$$

where A , B , C , n and m are material constants. Quasi-static tensile tests were performed, on an INSTRON 8801 universal testing machine at a loading rate of 3.6 mm/min (this corresponds to a nominal strain rate of $2 \times 10^{-3} \text{ s}^{-1}$) to obtain the strain hardening parameters (A , B and n). At least three tests were conducted to confirm the repeatability of the experimental data. The other material parameters, viz. rate dependency C and temperature m , were obtained from the published literature [33]. Table 4 lists the aforementioned parameters for the 304 steel that were used in the numerical simulations.

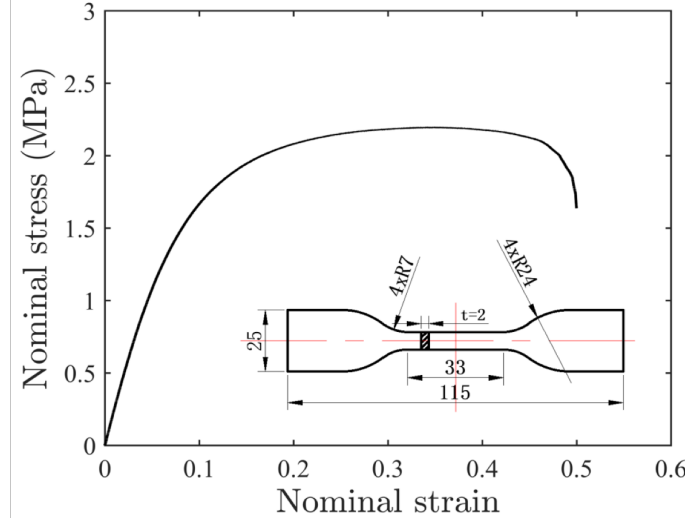
Table 4: Material properties and Johnson-Cook model parameters for the 304 stainless steel plate.

ρ	E	G	A	B	n	C	m
(kg/m ³)	(GPa)	(MPa)	(MPa)	(MPa)			
7830	210	80.8	283	1481	0.72 [33]	0.01 [33]	0.669 [33]

The polyurea coating is modeled as a hyperelastic rubber-like material. The well-established Mooney-Rivlin material model has shown to be a reasonably good representation of the



(a)



(b)

Figure 5: Nominal quasi-static stress-strain curves for the (a) 304 stainless steel plate, and (b) polyurea coating. All dimensions are in mm.

stress-strain relationship of polyurea and has been commonly used to model the constitutive behaviour of the polyurea material in high strain rate loading conditions, such as impact and blast [23–25, 34]. The Mooney-Rivlin material model describes the mechanical response by a strain energy function with respect to the strain invariants of the left Cauchy–Green tensor. Here, an incompressible, two parameters, Mooney-Rivlin hyperelasticity material model was used. It has a strain energy density W expressed as a function of the strain invariants given by

$$W = C_{10}(I_1 - 3) + C_{01}(I_2 - 3) \quad (2)$$

where C_{10} and C_{01} are the material constants; I_1 and I_2 are the first and second invariants of right Cauchy-Green tensor. Here, the parameters C_{10} and C_{01} were determined by fitting Eq. 2 to the quasi-static tensile test data shown in Fig. 5b, and they are listed in Table 5. Again, at least three tests were conducted to confirm the repeatability of the experimental data in Fig. 5b. Note that, the current Mooney-Rivlin material model does not consider the strain rate sensitivity of the polyurea, which only incorporates an individual strain rate. Notwithstanding, quasi-static tensile test data were often used with excellent fidelity [23, 35] and was also used here.

Table 5: Material properties and Mooney-Rivlin model parameters for polyurea.

Density ρ (kg/m ³)	Poisson's ratio ν	C_{10} (MPa)	C_{01} (MPa)
1020	0.486	4.20	7.57

3.4. Numerical results

3.4.1. Out-of-plane deflection and blast overpressure

Figure 6 compares the temporal central (out-of-plane) deflection $w_0(t)$ predicted by FE to their experimental counterpart. A summary of the predictions are tabulated and compared in Table 6. The FE model successfully predicts the overall mode I elasto-plastic response of both the monolithic and laminate plates. The temporal histories $w_0(t)$ agree reasonably well with their experimental counterpart for all the target configurations, except for P-S-P where FE over-predicts the time it took to reach the maximum out-of-plane displacement w_0^{\max} . The reason is unclear and could be due to the stochastic nature of imperfection of the blast tests. The model also slightly underestimates the maximum out-of-plane deflection (w_0^{\max}) by an average of 9.31%. This can be attributed to after-burning – it has the typical effect of enhancing the confined blast load [13] – which was not considered in the current FE model.

Table 6: Summary of predictions for different target configurations.

Test number	Mass of TNT charge (g)	Target structure	Peak transient deflection w_0^{\max} (mm)		Impulse saturation time t_{Sat}^I (ms)	Saturated impulse I_{Sat} (N·s/m ²)
			Experiment	FE	FE	FE
1	10	S	22.12	20.18	0.9	327.7
2	10	P-S	33.76	30.06	1.13	345.8
3	10	S-P	33.30	29.45	1.13	345.8
4	10	P-S-P	31.61	29.72	1.14	350

P, S stands for polyurea and steel, respectively.

In Fig. 6, the predicted time-history of the average blast overpressure $p(t)$ (solid red lines) is plotted to reveal the loading characteristics from the confined blast. Note that the average

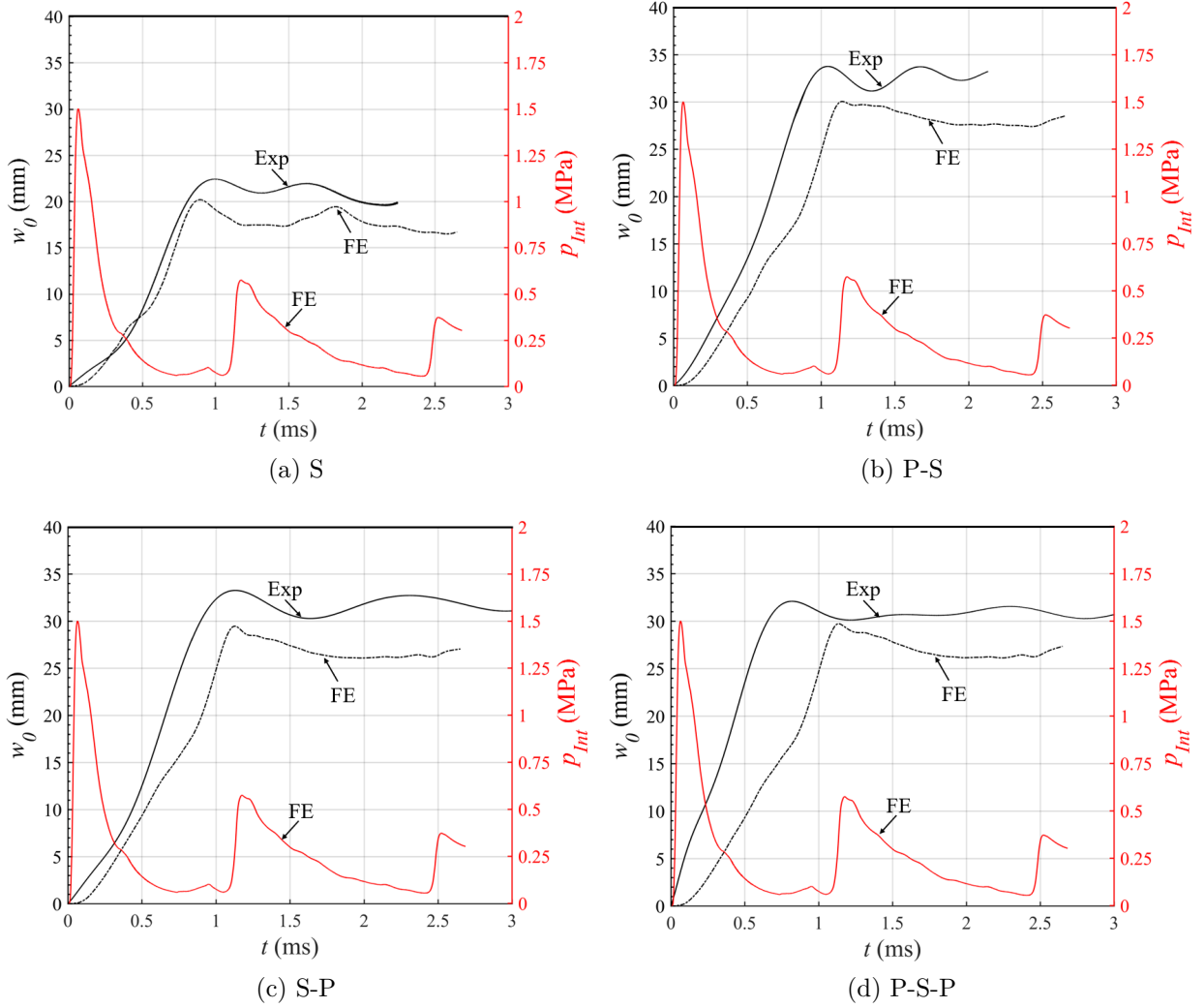


Figure 6: Temporal history of the predicted central (out-of-plane) deflection $w_0(t)$ against corresponding experimental data for different target configurations.

blast overpressure provides a measure of the overall intensity of the blast load. It is evident from the local overpressure contour plot of the target-air interface, see Fig. 7, that the blast overpressure is non-uniform during the fluid-structure interaction. For instance, the blast overpressure is highest near the corners of the plate at $t = 0.08$ ms but evolve towards the central region at $t = 0.15$ ms. The overpressure curves in Fig. 6 exhibit traits that are typical of a confined blast, i.e. multiple overpressure spikes with a significant loading duration. Despite the considerable loading duration (≥ 2.5 ms) compared to its external counterpart of the same charge mass at the same standoff (≈ 0.5 ms), the out-of-plane deflection of the plate does not increase without bound; instead, it reaches a maximum value w_0^{\max} fairly early in the loading phase (corresponding to 0.9, 1.13, 1.13 and 1.14 ms for S, P-S, S-P and P-S-P, respectively, in Fig. 6 and Table 6). The reason for this is that membrane

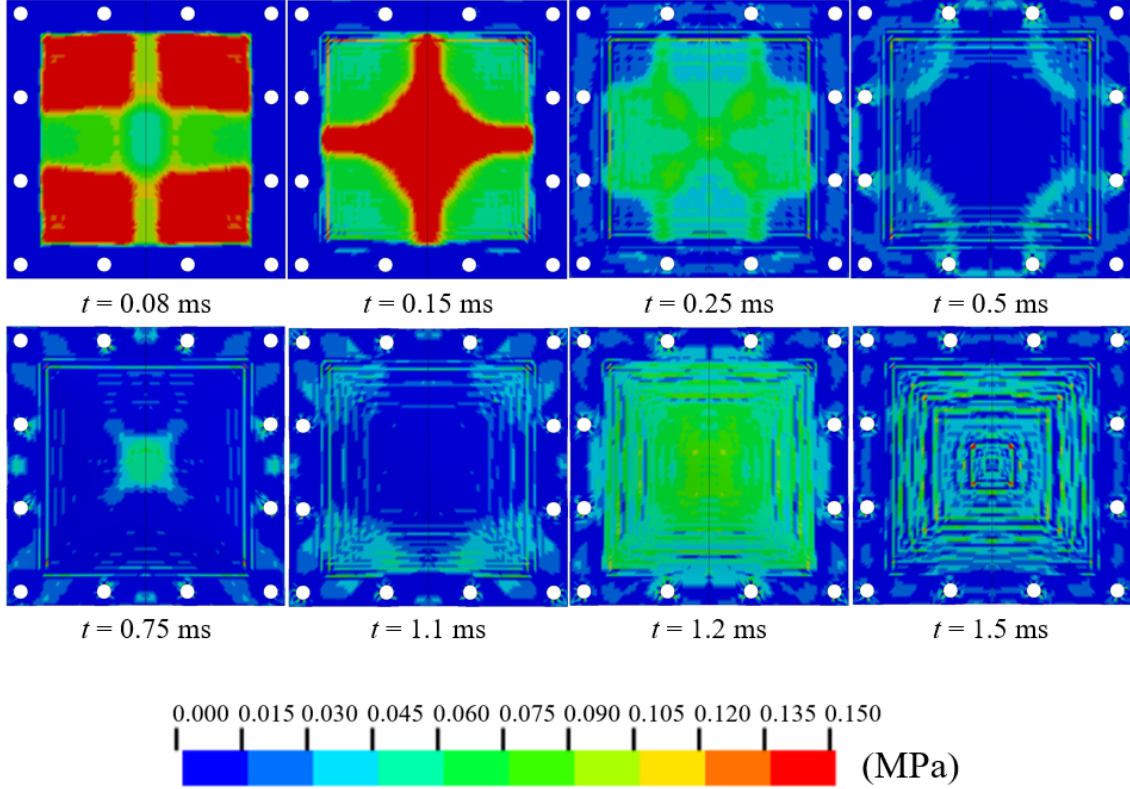


Figure 7: Temporal evolution of the local blast overpressure distribution at the target-air interface for a P-S target plate predicted by FE.

230 action can strengthen the structure to a point where the blast load fails to induce further
 231 additional inelastic deformation. This is known as an impulse saturation phenomenon [36]
 232 – its importance to the mode I response of monolithic plates to confined blast loading was
 233 recently highlighted by Yuan et al. [4]. The time taken for the central plate deflection to
 234 reach its maximum value, referred to as the saturation time t_{Sat}^I , is given by

$$\dot{w}_0(t = t_{\text{Sat}}^I) = 0', \quad (3)$$

235 and the corresponding total impulse transmitted to the plate at saturation (known as the
 236 saturated impulse I_{Sat}) is

$$I_{\text{Sat}} = \int_0^{t_{\text{Sat}}^I} p_{\text{Int}}(t) dt. \quad (4)$$

237 Both are important parameters when evaluating the blast performance of the structures,
 238 since the former is directed related to the latter.

239 In general, it was found that the laminate plates have a longer impulse saturation time t_{sat}^I
 240 (25.6% greater) compared to its monolithic counterpart as shown in Fig. 6 and Table 6. In
 241 other words, by the time a monolithic steel plate reaches its maximum central displacement
 242 at $t = 0.9$ ms, and begins the process of elastic rebound, the central out-of-plane deflection

of the laminate plates is still increasing. Hence, the increased deformation is a result of replacing a proportion of the steel plate with a polyurea coating – recall that comparisons were made for plates of equal mass.

3.4.2. Energy partitioning

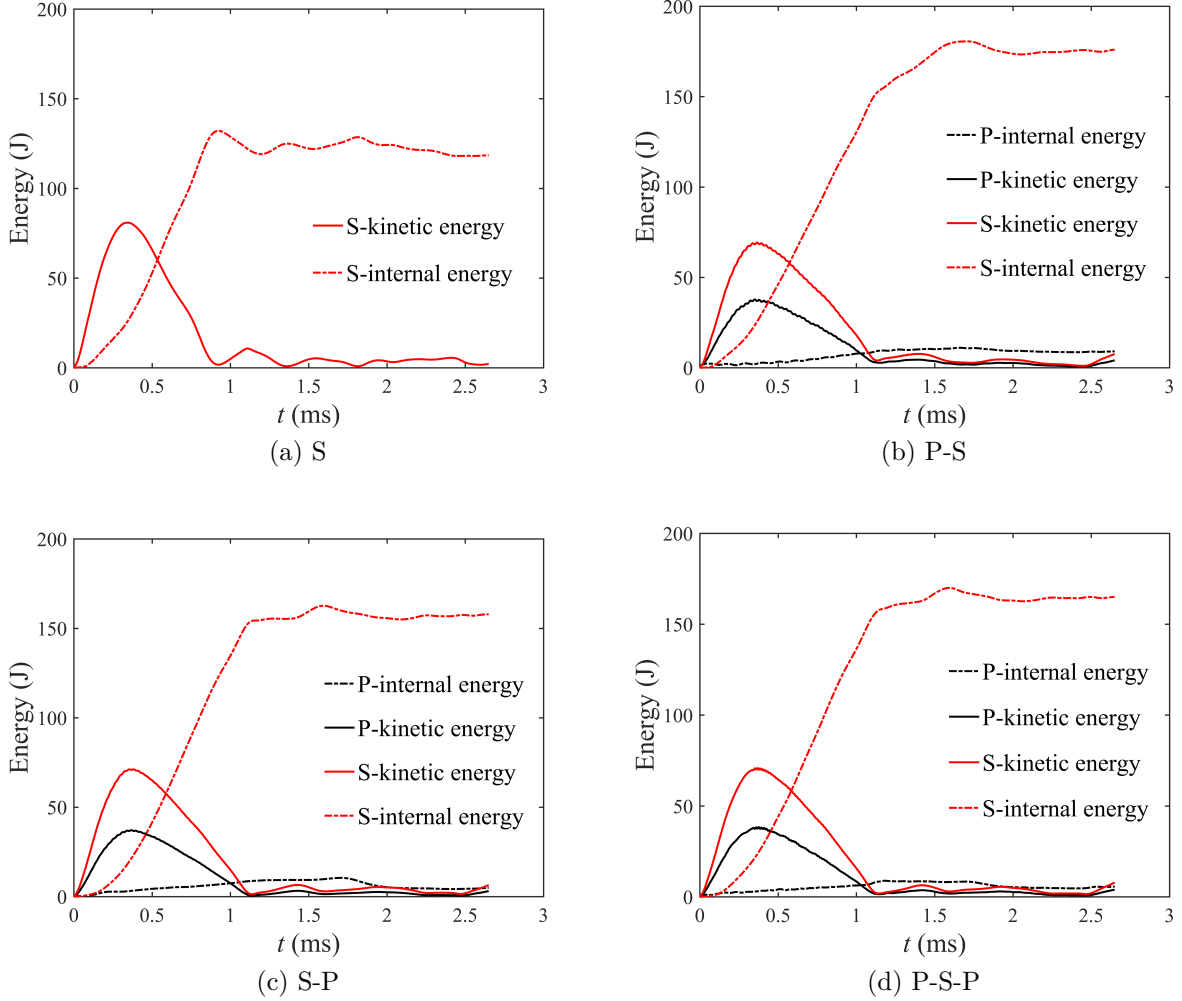


Figure 8: Temporal history of the partitioned energy for the different target configurations predicted by FE.

By replacing a fraction of the original monolithic steel plate ($\approx 39.4\%$) with polyurea of the same mass, the effective resistance to out-of-plane deformation is lowered for the resulting laminate plate compared to its monolithic steel counterpart. This is due to the massive strength (of approximately two orders of magnitude) mismatch between steel and polyurea as shown in Fig. 5. Figure 8 plots the temporal variation of the kinetic (solid lines) and internal (dash lines) energies of the steel and polyurea layers (steel in red and polyurea in black) for the different target configurations. In general, the internal (or strain) energy of the polyurea coating is insignificant compared to its steel substrate for all the laminate configurations,

see Figs. 8b-8d. Comparing Figs. 8b-8d to Fig. 8a, the first peak total kinetic energy of the laminate plates (S-P, P-S and P-S-P) are higher than its monolithic steel counterpart (S) ($\approx 34.4\%$) which implies that the former acquires a higher velocity in the early phases of their FSI response even though both have identical mass - this a direct consequence of their lower resistance to out-of-plane deformation. The additional kinetic energy acquired by the polyurea-steel laminate plates is dissipated through the internal (or strain) energy, the majority of which through the steel substrate rather than the polyurea-coating. This explains the deformation increase for the polyurea-steel laminate plates observed in the experiments.

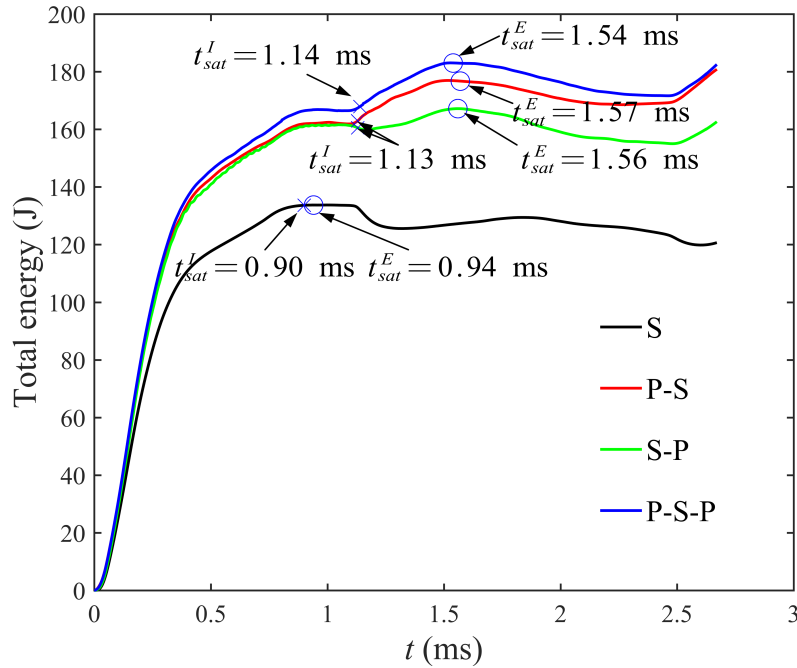


Figure 9: Temporal history of the total energy for different target configurations.

The time-histories of the total energy (kinetic plus internal) are plotted in Fig. 9. It is unsurprising that the total energy of the monolithic steel (S) plate is lower than its laminate equivalents (S-P, P-S and P-S-P) because a higher impulse is transmitted during FSI to the latter due to its lower flexural resistance. The impulse saturation time t_{sat}^I for each configuration is also indicated. Here, the time instant corresponding to maximum total energy is defined as the energy saturation time t_{sat}^E , as shown in Fig. 9. It is interesting to note that, for the monolithic steel plate, $t_{sat}^E=0.94$ is only slightly higher than $t_{sat}^I=0.9$, implying that the monolithic steel plate stops absorbing energy as soon as its central displacement reaches a maximum. By contrast, there is a notable time difference between t_{sat}^I and t_{sat}^E for the polyurea-steel laminate plates. In other words, the laminate plates must continue to deform inelastically even after their maximum central deflection is reached.

To verify the above, the temporal evolution of the average and central velocities of the

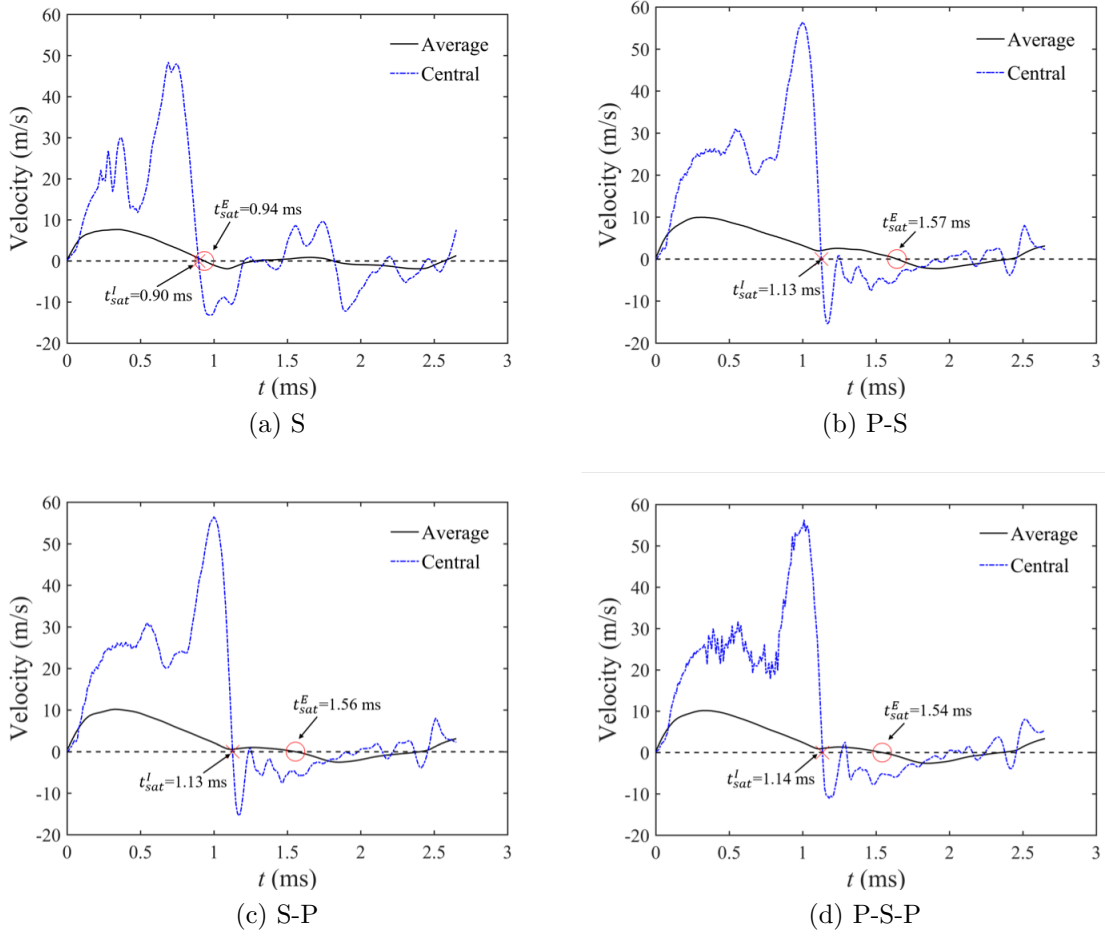


Figure 10: FE predictions of the average and central velocities for different target configurations.

plates were plotted in Fig. 10. The impulse t_{sat}^I and energy saturation time t_{sat}^E are also indicated, which appears to coincide, rather surprisingly, with the time instants at which the average velocity v_{ave} and central velocity v_0 first drop to zero. In the laminate plates, when motion ceases at its mid-point (or central location) at t_{sat}^I , just before the beginning of elastic rebound, the rest of the structure continues to deform in its original z -direction; this is evident from the positive average velocity during the interval between $t_{\text{sat}}^I \leq t \leq t_{\text{sat}}^E$. The average blast overpressure during this time interval, as shown in Fig. 6, reveal that the plates are still under the influence of a second round of pulse-pressure loading arising from the confinement, and this is responsible for the further increase of deflection (for the rest of the structure besides the mid-point) and internal energy.

Figure 11 shows the temporal evolution of the out-of-plane deformation profile of the monolithic steel and P-S laminate plates. Since the polyurea coating is perfectly bonded to the steel substrate, the deformation profile of the steel substrate is plotted here to represent the laminate plate. In the early stages ($t = 0.3$ ms in Fig. 11a and $t = 0.5$ ms in Fig. 11b),

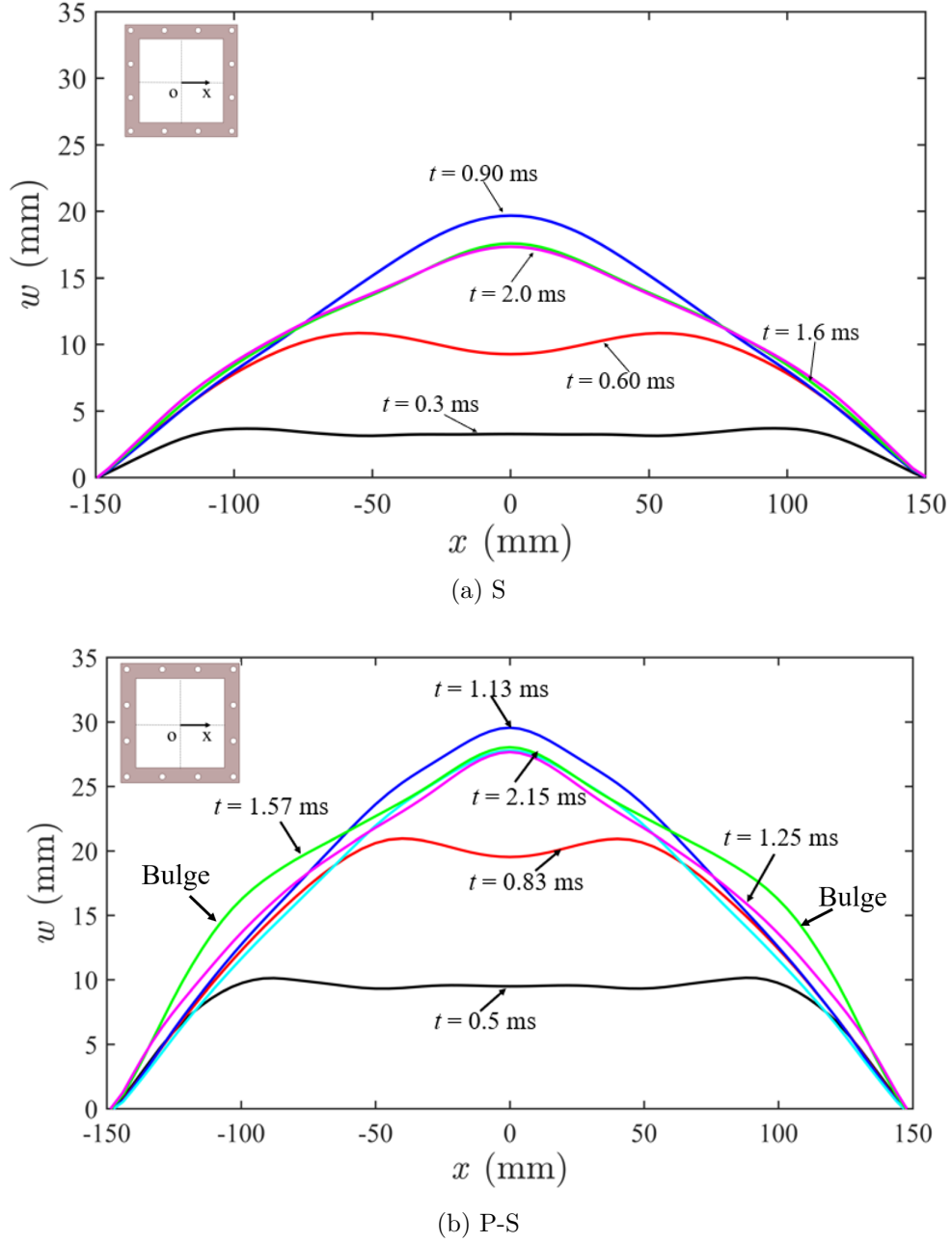


Figure 11: Predictions of the length-wise deformation profile, through the midspan, for different target configurations by FE: (a) S and (b) P-S.

290 plastic hinges (or, more accurately, lines) form at the vicinity of the boundary leaving a
 291 relatively flat central region in the middle of the plate. With time (see $t = 0.6$ ms in Fig.
 292 11a and $t = 0.83$ ms in Fig. 11b), the aforementioned central region begins to shrink while
 293 its central deflection continues to increase. At the impulse saturation time ($t_{\text{sat}}^I = 0.9$ ms in
 294 Fig. 11a and $t_{\text{sat}}^I = 1.13$ ms in Fig. 11b), both the monolithic and laminate plates acquire

a pyramidal profile - the same were also observed experimentally in all-metal square plates subjected to a confined blast [2]. However, at the energy saturation time of $t_{\text{sat}}^E = 1.57$ ms, two local bulges ($-150 \leq x \leq -50$ and $50 \leq x \leq 150$ in Fig. 11b) form in the laminate plate which is absent in their monolithic equivalent in Fig. 11a. Figure 11b confirms that the internal energy of a laminate plate can continue to increase, through further out-of-plane deformation that spreads laterally, such as the one shown above, even if it has reached its maximum central displacement - this is consistent with the previous results shown in Figs. 9 and 10.

3.5. Interface pressure

Figure 12 shows the pressure variation on the steel-polyurea interface at selected times for different target configurations. The first and third time instants refer to the time when blast overpressure reaches its maximum in Fig. 6a and the impulse saturation time t_{sat}^I , respectively. For the P-S-P configuration, the interface pressure on the front and rear coating are shown in Fig. 12d. It is clear that the polyurea coating has a significant effect in modifying the interfacial pressure experienced by the steel substrate - by inducing localised regions of high and low pressure fluctuations - and, consequently, on its out-of-plane deformation profile and the concomitant energy that was absorbed. At the first frame, loading acting on the monolithic steel plate (Fig. 12a) is significant; however for the polyurea-coated steel plates, the frontal layer (polyurea coating or steel substrate) is effective to attenuate the transmitted load resulting in an interface pressure field with low intensity - this will be confirmed later in Fig. 13. After $t \geq 0.6$ ms, the pressure distribution on the monolithic steel plate (Fig. 12a) is nearly uniform unlike its laminate counterparts (Figs. 12 b-d). Even though the laminate plates (P-S, S-P and P-S-P) have reached their maximum out-of-plane central displacement at $t = t_{\text{sat}}^I$ (third column), there remains considerable pressure acting on their steel substrate. For the P-S-P configuration in Fig. 12d, the interface pressure acting on the front central region (facing the incoming blast) is greater than its corresponding rear surface. However, the opposite to the aforesaid occurs near the boundary since there is more severe localisation of the interface pressure near the boundary on the rear surface of the steel layer.

Figure 13 presents the average interface pressure as a function of time for the different configurations. The interface pressure acting on the monolithic steel configuration is, unsurprisingly, identical to the average blast overpressure plotted in Fig. 6a, and it will be used as a benchmark to establish whether the interface pressure is amplified, or attenuated, by the presence of a polyurea coating. Figure 12 already shows that the huge impedance mismatch between polyurea and steel, and the location of the polyurea coating, relative to the direction of loading, has a significant effect on the distribution of the interface pressure. Attenuation of the interface pressure is clearly evident in the polyurea-coated steel plates in their early stages of deformation ($t < 0.3$ ms), irrespective of the location of coating. Between $0.3 \leq t \leq 1.2$ ms, the interface pressure acting on the P-S, S-P and P-S-P exceeds that of the blast overpressure. Following the arrival of the secondary blast at $t = 1.2$ ms, attenuation is, again, achieved at the interface of the P-S and P-S-P (the rear ones)

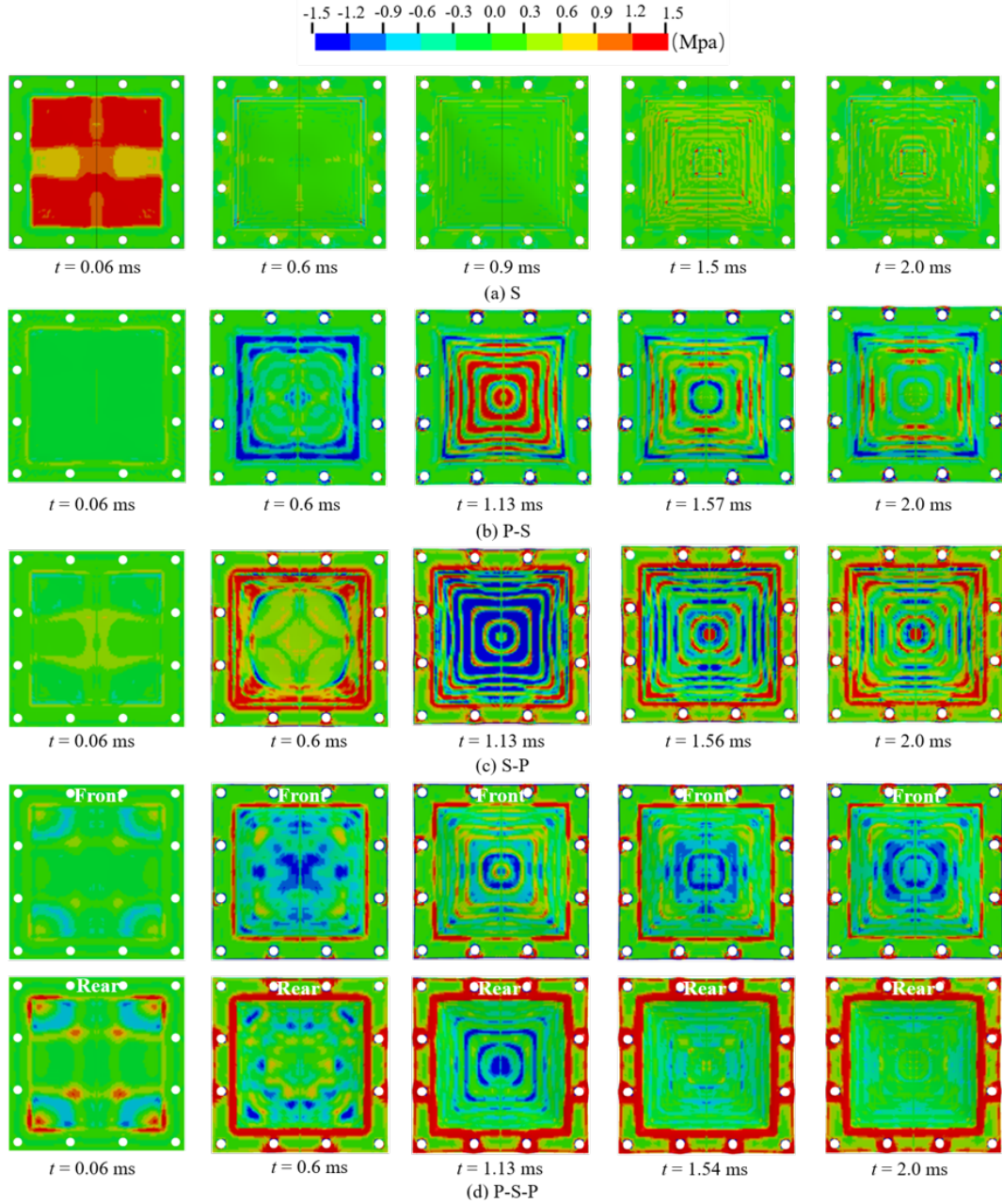


Figure 12: Contours of interface pressure on the steel substrate at selected times for the different target configurations predicted by FE.

plates. However, in the S-P configuration, the interface pressure is amplified, where the absolute value of the peak pressure (0.87 MPa) exceeds that caused by the secondary blast wave (0.57 MPa). Table 7 compares the peak interface pressure between the two different phases (primary and secondary) of loading for different target configurations. With the notable exception of the S-P configuration, the peak interface pressure experienced by the steel substrate (of the laminate plates) is always lower than the corresponding primary and

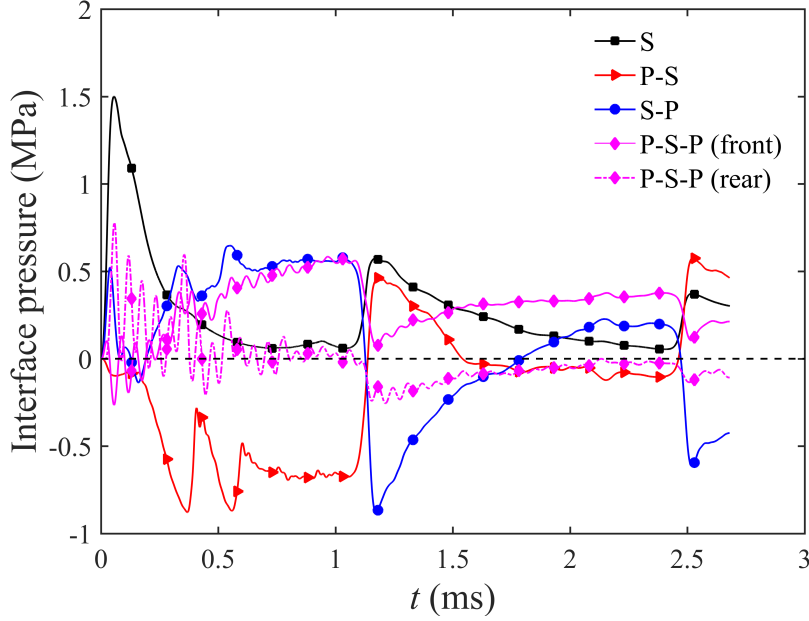


Figure 13: Average interface pressure on the steel substrate predicted by FE for different target configurations.

secondary blast overpressure impinging on the plate, i.e. the polyurea coating has the effect of attenuating the blast load.

Table 7: Comparison of the peak interface pressure between the different configurations.

Target configuration	Absolute value of peak interface pressure (MPa)	
	Primary blast loading ($0 \leq t \leq 1.2$ ms)	Secondary blast loading ($1.2 \leq t \leq 2.5$ ms)
S	1.50	0.57
P-S	0.88	0.46
S-P	0.65	0.87
P-S-P (front)	0.58	0.38
P-S-P (rear)	0.78	0.25

3.6. Equivalent plastic strain

Equivalent plastic strain is a critical parameter to estimate the possible location of fracture for the metallic structure under blast loading [37]. Figure 14 shows the equivalent plastic strain contour of the steel substrate in the different configurations. The contours correspond to the instant of maximum out-of-plane central displacement in each case. For both the monolithic and polyurea-coated steel plates, the equivalent plastic strain is either highly localised in the central region of the plate or in the vicinity of the bolt holes along the

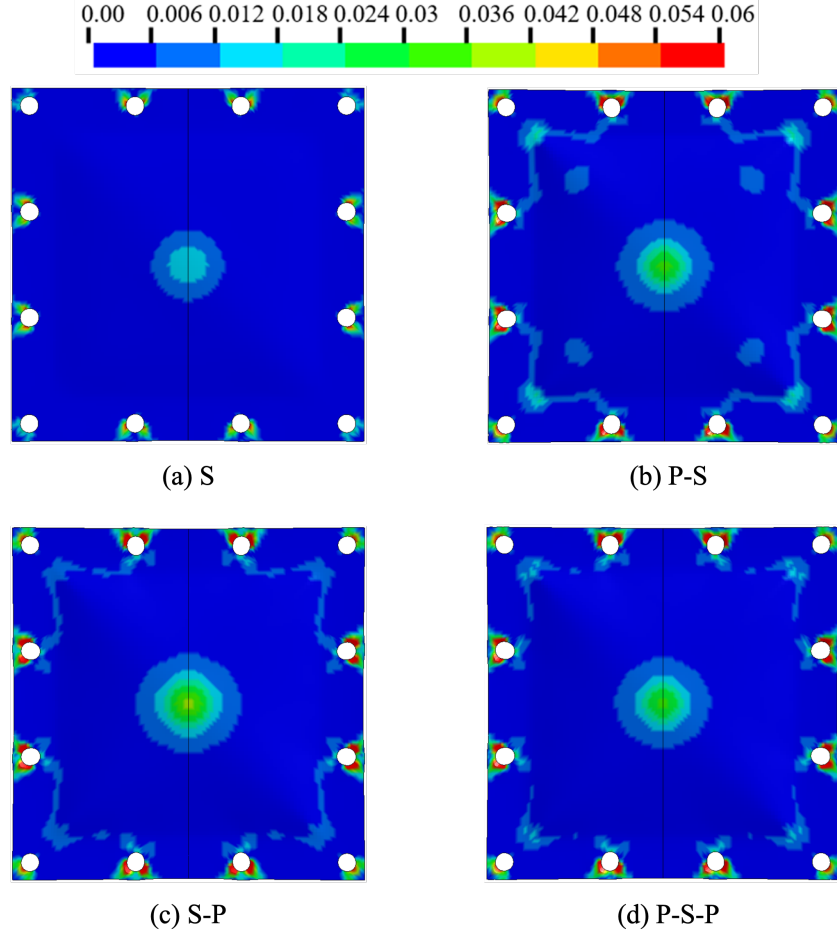


Figure 14: Equivalent plastic strain contour of the steel layer in the different configurations.

boundary. The latter is more localised, with a higher equivalent plastic strain, compared to the former. Slight distortion of the circular bolt holes were observed – this is due to ‘pull-in effect’ – which increases the out-of-plane deflection of thin plates caused by insufficient clamping force along the plate boundary [2]. Previous studies [19, 29] reported that cracking initiates, and grow circumferentially, near the centre of the polyurea-steel laminate plates when subjected to impulsive loadings. Although Fig. 14 shows that localisation of deformation is indeed present in the central plate region, the equivalent plastic strain contour indicates that fracture is likely to initiate from the bolt holes instead if the confined blast loading is sufficiently intense. This was also observed in experiments, [38] and predicted by finite element simulations [39], for fully-clamped monolithic metal plates under uniformly distributed air-blast loading in the literature.

3.7. Effects of thickness ratio and area density

Parametric studies were performed to evaluate the sensitivity of the maximum central deflection by the laminate plate to its area density and the thickness ratio of polyurea to

steel layer. In the first case, comparisons were made on an equal mass basis (or equal area density); whereas, in the second case, the equal mass constraint was relaxed so that the polyurea coating can be regarded as an added material to an existing steel structure, typically encountered during retrofitting.

The maximum central deflection, its area density and thickness ratio are non-dimensionalised as follows:

$$\bar{w} = \frac{w(t = t_{\text{Sat}}^I)}{a}, \quad \bar{\mu} = \frac{\rho_p h_p + \rho_s h_s}{\mu_0}, \quad \text{and} \quad \bar{h} = \frac{h_p}{h_s} \quad (5)$$

where $a = 150$ mm is the half width of the exposed area to the blast; subscripts p and s denote polyurea and steel, respectively; and, $\mu_0 = 12.83$ kg/m² is the area density of the target plates. The following loading parameters were used in the simulations: 10g of TNT charge and 150 mm of standoff distance. And, the geometry of the blast chamber is identical to that in the current experiments. The exposed area of the square plate to the blast has identical length and width of $2a = 300$ mm. For simplicity, it will be assumed that both the polyurea layers in the P-S-P configuration have the same thickness.

Figures 15a-15c plots the variation of the dimensionless maximum central deflection \bar{w} as a function of the dimensionless area density $\bar{\mu}$ for a range of thickness ratio between $2 \leq \bar{h} \leq 6$. The prediction for a monolithic steel plate of equal mass was also included in each figure to compare the blast performance of monolithic and laminate plates. If \bar{w} is adopted as the criterion to assess blast performance, then it is clear that the monolithic plate outperform its laminate counterpart regardless of the location of the polyurea placement, for all the combinations of $\bar{\mu}$ and \bar{h} investigated here. In each figure, the gap between the curves of the monolithic and laminate plates diminishes with reducing thickness ratio \bar{h} . The monotonic reduction of \bar{w} with lower \bar{h} is attributed to the greater resistance offered by the thicker steel layer. For each target configuration, increasing the dimensionless area density $\bar{\mu}$ leads to a monotonic reduction of \bar{w} for each \bar{h} – this is consistent with the findings reported by Ackland et al. [24].

If spray-on polyurea is used to retrofit an existing structure, then the polyurea coating should be treated as an added mass to the steel substrate. Consequently, it is necessary to relax the *equal mass* constraint and to examine how the thickness ratio $\bar{h} = h_p/h_s$ affects the blast resistance for a constant thickness of the steel substrate. Figures 16a-16c show the variation of \bar{w} as a function of thickness ratio \bar{h} for a range of steel layer's thickness $1 \leq h_s \leq 2$. In general, a thicker steel substrate h_s or a higher thickness ratio \bar{h} would lead to a monotonic reduction of the non-dimensional deflection \bar{w} for the P-S, S-P and P-S-P configurations, with the notable exception of the S-P configuration where \bar{w} increases marginally from $\bar{h} = 0 - 2$ at $h_s = 1.5$ and 1.75 mm.

Lastly, it must be emphasised that all the results reported in Section 3.7 adopts \bar{w} as a criterion to assess performance and, more importantly, comparisons were made subject to the constraint of mode I deformation only. If, however, a different criterion is adopted and/or the target deforms in a different mode, then the above conclusion is likely to change.

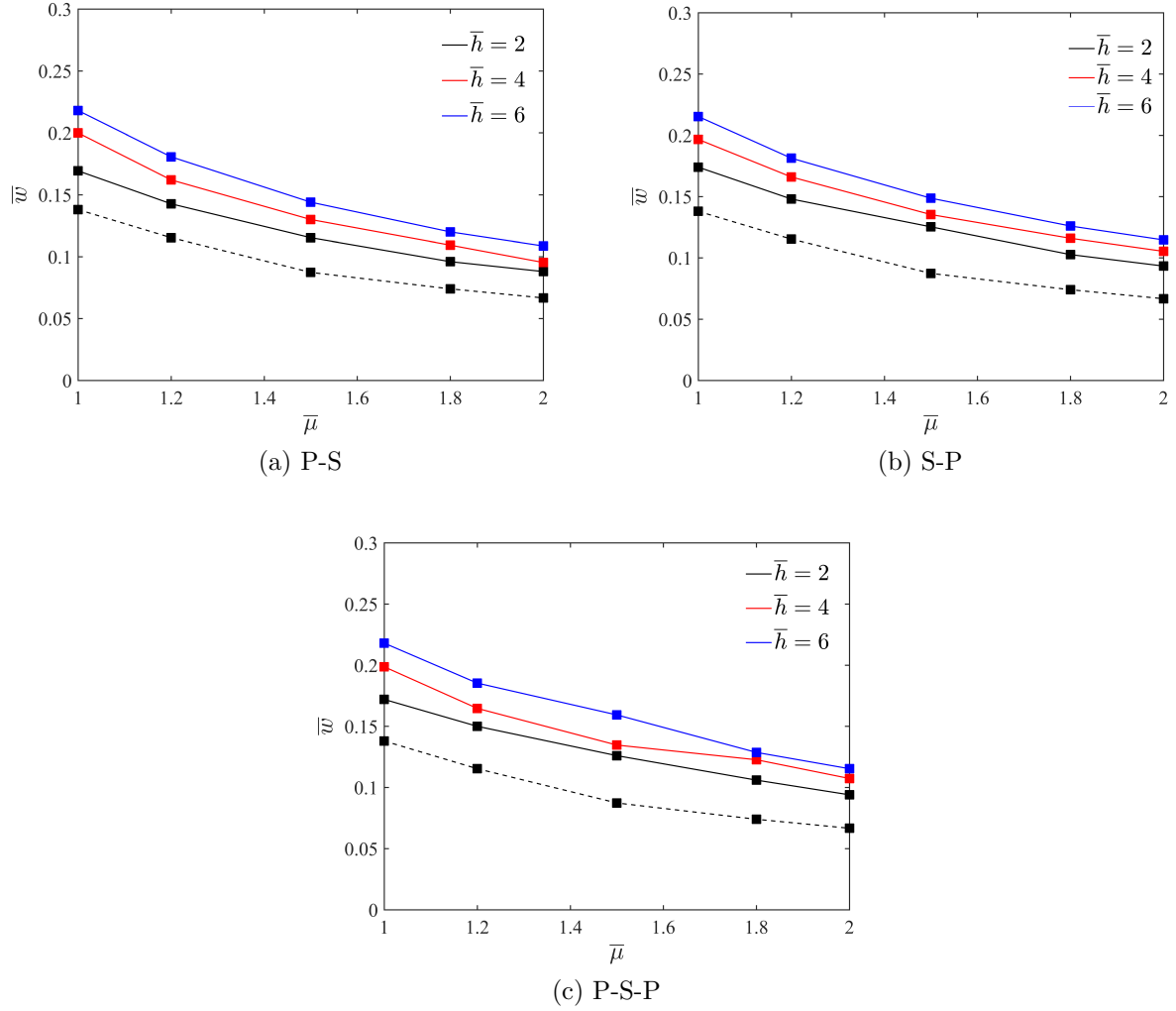


Figure 15: Variation of the non-dimensional maximum central deflection \bar{w} with non-dimensional areal density $\bar{\mu}$ at different thickness ratio \bar{h} for laminate plates (a) P-S, (b) S-P and (c) P-S-P. The predictions for monolithic steel plates having equal areal density $\bar{\mu}$ were also inserted in each figure as a black dotted line (- -).

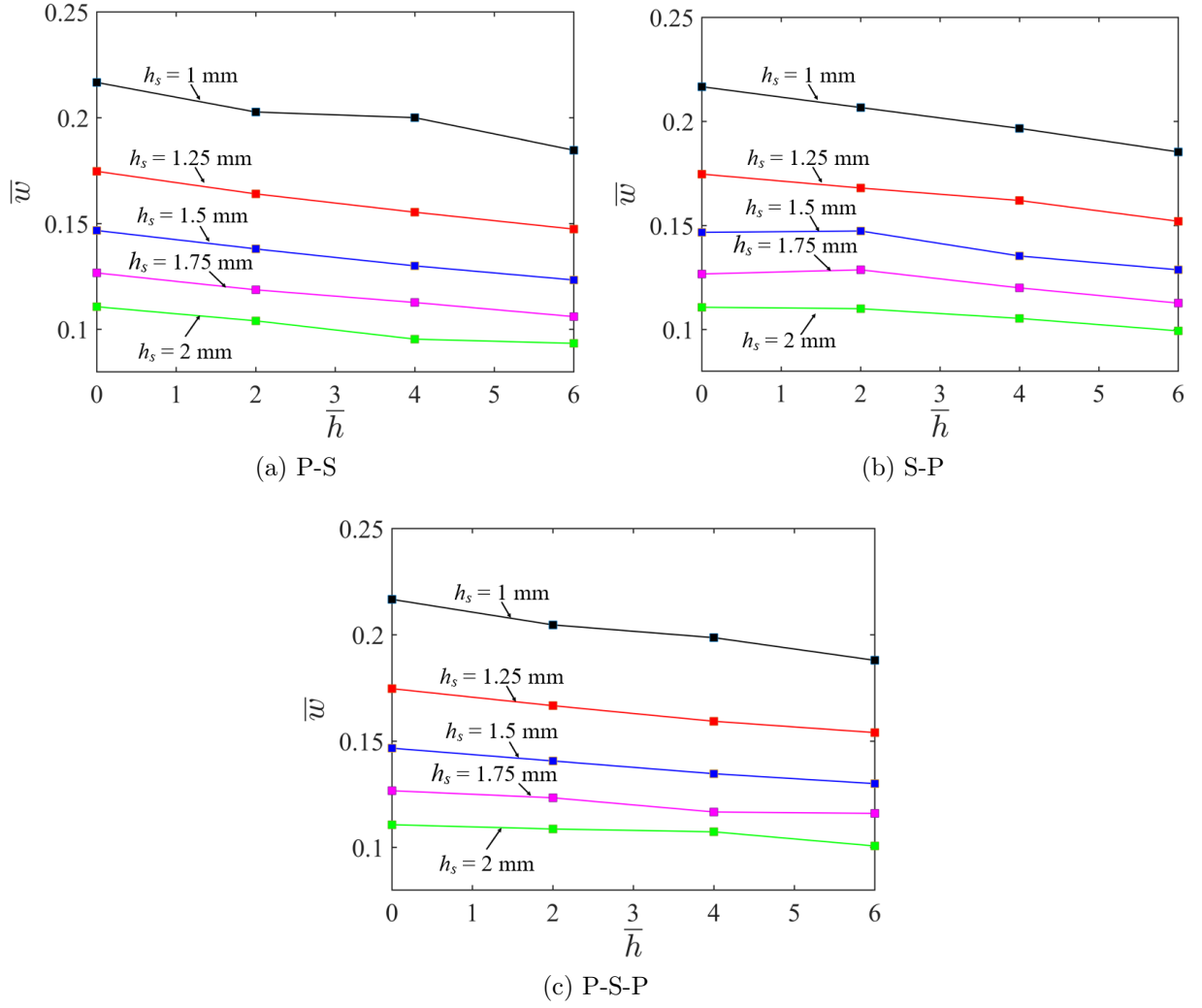


Figure 16: Variation of the non-dimensional maximum central deflection \bar{w} with non-dimensional thickness ratio \bar{h} at different thickness for steel layer (a) P-S, (b) S-P and (C) P-S-P.

4. Conclusion

Experiments and numerical FE modelling were performed to compare the mode I blast (confined) performance of polyurea-steel laminate plates and monolithic steel plates of equal mass. The following key conclusions can be drawn:

- A polyurea coating applied on either, or both, sides of a steel substrate did not lead to improved blast performance if the maximum central deflection is used as a criterion.
- The impedance mismatch between the steel and polyurea was shown to play a key role in re-distributing the interfacial pressure at the steel-polyurea interface, and it was demonstrated that the polyurea coating either amplifies or attenuates the blast wave depending on their placement relative to the substrate and the direction of loading.
- Results from the parametric study revealed that reducing the thickness ratio (polyurea to steel substrate), while keeping the total mass constant, leads to a reduction in the maximum central deflection of the laminate plate.
- The effectiveness of retrofitting the existing steel substrate with polyurea coating at different locations was also evaluated where it was found that a thicker polyurea coating would, in general, be beneficial in reducing the mode I central deflection of the laminate plate.

Acknowledgment

This research was financially supported by the National Natural Science Foundation of China [grant number 12102049] and the State Key Laboratory of Explosion Science and Technology, Beijing Institute of Technology [grant number QNKT22-02].

References

- [1] Langdon, G. S., Kriek, S., Nurick, G. N., [Influence of venting on the response of scaled aircraft luggage containers subjected to internal blast loading](#), International Journal of Impact Engineering 141 (2020) 103567.
- [2] Yuan, Y., Zhang, C., Xu, Y., [Influence of standoff distance on the deformation of square steel plates subjected to internal blast loadings](#), Thin-Walled Structures 164 (2021) 107914.
- [3] Zhang, C., Tan, P. J., Yuan, Y., Confined blast loading of steel plates with and without pre-formed holes, International Journal of Impact Engineering 163 (2022) 104183.
- [4] Yuan, Y., Li, X., Zhang, C., Tan, P., Chen, P., [Impulse saturation in metal plates under confined blasts](#), International Journal of Impact Engineering 168 (2022) 104308.
- [5] Hu, Y., Wu, C., Lukaszewicz, M., Dragos, J., Ren, J., Haskett, M., [Characteristics of Confined Blast Loading in Unvented Structures](#), International Journal of Protective Structures 2 (1) (2011) 21–43.
- [6] Duffey, T., Rodriguez, E., Romero, C., Detonation-induced dynamic pressure loading in containment vessels, Los Alamos national laboratory report LA-UR-02-0366.
- [7] Edri, I., Savir, Z., Feldgun, V., Karinski, Y., Yankelevsky, D., On blast pressure analysis due to a partially confined explosion: I. experimental studies, International Journal of Protective Structures 2 (1) (2011) 1–20.
- [8] Baker, W., Cox, P., Westine, P., Kulesz, J., Strehlow, R., Fundamental studies in engineering. Explosion hazards and evaluation, Vol. 5, Amsterdam, Oxford, New York: Elsevier, 1983.

- [9] Feldgun, V. R., Karinski, Y. S., Edri, I., Yankelevsky, D. Z., [Prediction of the quasi-static pressure in confined and partially confined explosions and its application to blast response simulation of flexible structures](#), International Journal of Impact Engineering 90 (2016) 46–60.
- [10] Dragos, J., Wu, C., Oehlers, D. J., [Simplification of fully confined blasts for structural response analysis](#), Engineering Structures 56 (2013) 312–326.
- [11] Wu, C., Lukaszewicz, M., Schebella, K., Antanovskii, L., [Experimental and numerical investigation of confined explosion in a blast chamber](#), Journal of Loss Prevention in the Process Industries 26 (4) (2013) 737–750.
- [12] Pickerd, V., Bornstein, H., McCarthy, P., Buckland, M., [Analysis of the structural response and failure of containers subjected to internal blast loading](#), International Journal of Impact Engineering 95 (2016) 40–53.
- [13] Langdon, G. S., Ozinsky, A., Chung Kim Yuen, S., [The response of partially confined right circular stainless steel cylinders to internal air-blast loading](#), International Journal of Impact Engineering 73 (2014) 1–14.
- [14] Geretto, C., Chung Kim Yuen, S., Nurick, G. N., [An experimental study of the effects of degrees of confinement on the response of square mild steel plates subjected to blast loading](#), International Journal of Impact Engineering 79 (2015) 32–44.
- [15] Li, Y., Zhang, L., Xiao, D., Zhao, T., Du, Z., Wu, W., Fang, D., [Experiment and numerical study on dynamic response of liquid cabin under internal blast loading](#), Thin-Walled Structures 145 (2019) 106405.
- [16] Yao, S., Zhang, D., Lu, F., Li, X., [Experimental and numerical studies on the failure modes of steel cabin structure subjected to internal blast loading](#), International Journal of Impact Engineering 110 (2017) 279–287.
- [17] Yao, S., Zhang, D., Lu, Z., Lin, Y., Lu, F., [Experimental and numerical investigation on the dynamic response of steel chamber under internal blast](#), Engineering Structures 168 (2018) 877–888.
- [18] Zheng, C., Kong, X., Wu, W., Xu, S., Guan, Z., [Experimental and numerical studies on the dynamic response of steel plates subjected to confined blast loading](#), International Journal of Impact Engineering 113 (2018) 144–160.
- [19] Amini, M. R., Isaacs, J. B., Nemat-Nasser, S., Experimental investigation of response of monolithic and bilayer plates to impulsive loads, International Journal of Impact Engineering (2010) 8.
- [20] Zhang, L., Ji, C., Wang, X., Wang, Y., Wu, G., Zhu, H., Han, Z., Strengthening and converse strengthening effects of polyurea layer on polyurea–steel composite structure subjected to combined actions of blast and fragments, Thin-Walled Structures 178 (2022) 109527.
- [21] Wang, X., Ji, C., Wu, G., Wang, Y., Zhu, H., [Damage response of high elastic polyurea coated liquid-filled tank subjected to close-in blast induced by charge with prefabricated fragments](#), International Journal of Impact Engineering 167 (2022) 104260.
- [22] Amini, M. R., Simon, J., Nemat-Nasser, S., [Numerical modeling of effect of polyurea on response of steel plates to impulsive loads in direct pressure-pulse experiments](#), Mechanics of Materials 42 (6) (2010) 615–627.
- [23] Chen, C., Wang, X., Hou, H., Cheng, Y., Zhang, P., Liu, J., [Effect of strength matching on failure characteristics of polyurea coated thin metal plates under localized air blast loading: Experiment and numerical analysis](#), Thin-Walled Structures 154 (2020) 106819.
- [24] Ackland, K., Anderson, C., Ngo, T. D., [Deformation of polyurea-coated steel plates under localised blast loading](#), International Journal of Impact Engineering 51 (2013) 13–22.
- [25] Hou, H., Chen, C., Cheng, Y., Zhang, P., Tian, X., Liu, T., Wang, J., [Effect of structural configuration on air blast resistance of polyurea-coated composite steel plates: Experimental studies](#), Materials & Design 182 (2019) 108049.
- [26] Mohotti, D., Fernando, P. L. N., Weerasinghe, D., Remennikov, A., [Evaluation of effectiveness of polymer coatings in reducing blast-induced deformation of steel plates](#), Defence Technology 17 (6) (2021) 1895–1904.
- [27] Samiee, A., Amirkhizi, A. V., Nemat-Nasser, S., [Numerical study of the effect of polyurea on the](#)

- performance of steel plates under blast loads, *Mechanics of Materials* 64 (2013) 1–10.
- [28] Chu, D., Wang, Y., Yang, S., Li, Z., Zhuang, Z., Liu, Z., [Analysis and design for the comprehensive ballistic and blast resistance of polyurea-coated steel plate](#), *Defence Technology* (2021) In press.
- [29] Amini, M. R., Isaacs, J., Nemat-Nasser, S., [Investigation of effect of polyurea on response of steel plates to impulsive loads in direct pressure-pulse experiments](#), *Mechanics of Materials* 42 (6) (2010) 628–639.
- [30] Amini, M., Amirkhizi, A., Nemat-Nasser, S., [Numerical modeling of response of monolithic and bilayer plates to impulsive loads](#), *International Journal of Impact Engineering* 37 (1) (2010) 90–102.
- [31] Menkes, S. B., Opat, H. J., [Broken beams](#), *Exp. Mech.* 13 (11) (1973) 480–486.
- [32] Nurick, G. N., Shave, G. C., The deformation and tearing of thin square plates subjected to impulsive loads—an experimental study, *Int J Impact Eng* 18 (1996) 99–116.
- [33] Zhao, N., Yao, S., Zhang, D., Lu, F., Sun, C., [Experimental and numerical studies on the dynamic response of stiffened plates under confined blast loads](#), *Thin-Walled Structures* 154 (2020) 106839.
- [34] Yuan, Y., Zhang, Q., Bian, X., Huang, G., Zhang, C., Su, X., Xu, Y., [Ballistic perforation resistance of elastomer-metal laminate plates](#), *Materials & Design* 224 (2022) 111434.
- [35] Liu, Q., Wang, S., Lin, X., Cui, P., Zhang, S., [Numerical simulation on the anti-penetration performance of polyurea-core Weldox 460 E steel sandwich plates](#), *Composite Structures* 236 (2020) 111852.
- [36] Zhu, L., Bai, X., Yu, T. X., [The saturated impulse of fully clamped square plates subjected to linearly decaying pressure pulse](#), *International Journal of Impact Engineering* 110 (2017) 198–207.
- [37] Yuan, Y., Tan, P. J., [Deformation and failure of rectangular plates subjected to impulsive loadings](#), *International Journal of Impact Engineering* 59 (2013) 46–59.
- [38] Aune, V., Fagerholt, E., Hauge, K., Langseth, M., Børvik, T., [Experimental study on the response of thin aluminium and steel plates subjected to airblast loading](#), *International Journal of Impact Engineering* 90 (2016) 106–121.
- [39] Aune, V., Valsamos, G., Casadei, F., Larcher, M., Langseth, M., Børvik, T., [Numerical study on the structural response of blast-loaded thin aluminium and steel plates](#), *International Journal of Impact Engineering* 99 (2017) 131–144.